THE JOURNAL OF PHYSICAL CHEMISTRY C

ARTICLE

pubs.acs.org/JPCC

Real-Space Investigation of Electrical Double Layers. Potential Gradient Measurement with a Nanometer Potential Probe

Young-Hwan Yoon, Dae-Ha Woo,† Taeho Shin, Taek Dong Chung,* and Heon Kang*

Department of Chemistry, Seoul National University, Gwanak-gu, Seoul 151-747, Republic of Korea

S Supporting Information

ABSTRACT: We report measurement of the potential gradient in a nanometer gap between a Au(111) electrode and a gold tip immersed in a $NaClO_4$ solution. A miniaturized potential probe, constructed with a gold tip and an insulator film, oscillates perpendicular to the electrode surface with a small amplitudes and measures the potential gradient in the local solution environment. The potential gradient is measured as a function of gap distance and then integrated over the distance to obtain the interfacial potential profile. When the probe is located far from the electrode surface, the interfacial potential profile decays exponentially with distance, similarly to the potential distribution of an isolated electrical double layer (EDL). At close gap distances, the profile exhibits an inflection point and a sigmoidal bending toward the electrode potential, which might differ somewhat from that of the isolated electrode surface. These features can be attributed to the overlap of the EDLs on the probe and electrode surfaces during the measurement and also to the electron tunneling between the two surfaces at very short distances. It is demonstrated that the potential gradient method detects signals originating exclusively from the interfacial potential component, whereas it effectively filters out time-dependent noises and potential drifts that might be associated with the complicated microscopic structure of the probe apex. This method can measure the potential profile width more accurately than a direct potential reading method, although it cannot quantitatively measure the absolute potential height.

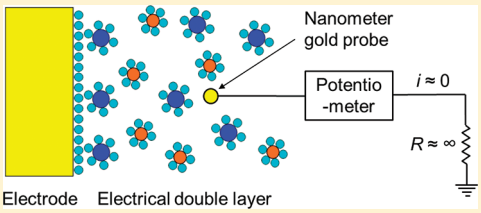

1. INTRODUCTION

The electrical double layers (EDLs) present at electrolyte/electrode interfaces play an important role in electrochemistry and colloidal science. Since the structure of the EDL was proposed in the early 20th century by Gouy,[1] Chapman,[2] and Stern,[3] observation of the EDL structure has been the focus of decades of experimental research.[4] Electrochemical studies have measured the capacitance of the EDL and the excess charge on electrode surfaces.[4] Real-space investigation of the EDL structure was first performed using a surface force apparatus[5,6] and then an atomic force microscope (AFM) by attaching a silica colloidal particle to the AFM tip.[7−9] These experiments measured the electrostatic forces present between the EDLs formed at the electrode and probe surfaces in close proximity, from which the thickness of a diffuse double layer was estimated.

A key feature that characterizes electrode/electrolyte interfaces is the electrical potential distribution inside the EDL. However, the EDL potential has been deduced mostly from theoretical studies and indirect experimental observations,[4−9] until several research groups recently initiated experiments to measure the EDL potential profile in real space.[10−14] Woo et al.[13] employed a nanometer gold tip as a potential sensor and a high-impedance potentiometer to monitor the interfacial potential profile of a Au(111) electrode immersed in a $NaBF_4$ solution. They observed that the interfacial potential changed as the tip moved toward the electrode surface across the EDL region and that the measured potential profile varied with the electrode bias potential, as expected. Hurth et al.[14] examined the interfacial potential profile of Pt foil and SiO_2/Si surfaces in dilute KCl solutions, by preparing a Pt−Ir tip coated with a polyethylene film and electrodeposited with silver at the tip apex. The application of such EDL potential measurements using a nanometer probe could be diverse, including scanning electrochemical potential microscopy (SECPM) for mapping the electrochemical potential of surfaces, as has been demonstrated by Corbella et al.[10] for diamond-like carbon films and by Baier and Stimming[11] for imaging a single enzyme on a graphite electrode.

Although the nanometer potential probe offers the possibility to monitor the potential of electrolyte/electrode interfaces, potential measurement with these probes does not reveal the potential distribution of the EDL at the electrode in a straightforward manner.[13,14] This is mainly because a miniaturized potential sensor prepared in the form of a tiny metal tip surrounded with an insulator sheath cannot be an ideal probe. The ideal potential probe would, by definition, be in perfect electrochemical equilibrium with the solution, and thus, no EDL should appear on the probe surface. Such a device would be able to monitor the potential of the EDL at the electrode surface without disturbing the EDL structure. However, this might not be possible in ordinary experiments. A nanometer-sized metal tip immersed in a solution usually carries an EDL on its surface as it reads the potential of the solution through a potentiometer,[15] and this

Received: March 8, 2011
Revised: July 15, 2011
Published: August 03, 2011

ACS Publications © 2011 American Chemical Society

EDL will interact with the EDL on the electrode surface being investigated. Recent theoretical studies[16,17] strengthen this objection by showing that the interfacial potential measured in SECPM experiments results from the overlap of the EDLs at the electrode and probe surfaces. In addition, it is difficult to characterize the nanoscopic structure of a potential probe constructed with a metal apex and an insulator sheath within the working environment of an electrochemical cell. The complicated structure of the probe could introduce various intervening effects into the potential measurement.[18] Apparently, there remain some important issues and technical barriers that need to be overcome for any real-space investigation of the EDL potential, and this requires new developments in experimental methods, as well as theoretical models of the EDL to understand the experimental results. In this article, we report the measurement of the potential gradient of electrolyte/electrode interfaces by using a gap-distance modulation method. This new method can remove some problems associated with the use of a nanometer potential probes constructed with a metal tip and an insulator film, and thus, it improves the reliability in profiling the interfacial potential.

2. EXPERIMENTAL SECTION

The experimental concept is illustrated in Figure 1a, which shows a cartoon corresponding to EDL potential measurement with an ideal potential probe. The potential distribution of the EDL at an electrode is monitored by using a small piece of metal, whose size is sufficiently smaller than the decay length of the EDL, as a potential sensor. The probe is placed near the electrode and moved perpendicular to the electrode surface to profile the EDL potential distribution. Alternatively, the probe is oscillated back and forth in small amplitudes to measure the potential gradient of the EDL. The ideal potential probe would measure the potential and potential gradient of the EDL without disturbing the EDL structure. In real experiments, however, the probe also carries an EDL on its own surface,[15−17] as mentioned above. In this case, the EDLs at the probe and electrode surfaces will interact with each other during the potential measurement. The measured potential profile will represent the potential distribution in the gap between the probe and electrode that results from the overlap of the two EDLs.

Figure 1b shows a schematic diagram of the experimental setup. It consisted of an electrochemical cell, a potential probe, a potentiometer, and an electrochemical scanning tunneling microscope. The electrochemical cell was composed of three electrodes; the working electrode (WE) was a Au(111) film deposited on glass, and the counter and reference electrodes (CE and RE) were also gold. Because a gold electrode was a quasireference electrode, a Ag/AgCl electrode (in saturated KCl) was occasionally used as an RE to compare the observed potentials with the reported values. The WE surface was annealed with a hydrogen flame,[19] which widened the (111) terrace area of the Au film, as verified by scanning tunneling microscopy (STM). The electrode potentials were controlled by a bipotentiostat (Pine model AFRDE5). The WE and RE potentials were separately controlled with respect to the ground in this configuration. The probe was an electrochemically etched gold wire coated with an insulating layer of nitrocellulose varnish except for its apex.[20] The potentiometer read the probe potential with respect to the laboratory ground, electrically separated from the bipotentiostat circuit. The electrolyte solution contained $NaClO_4$ at various concentrations in doubly distilled, deionized water. It is reported that Na^+ and ClO_4^- ions have

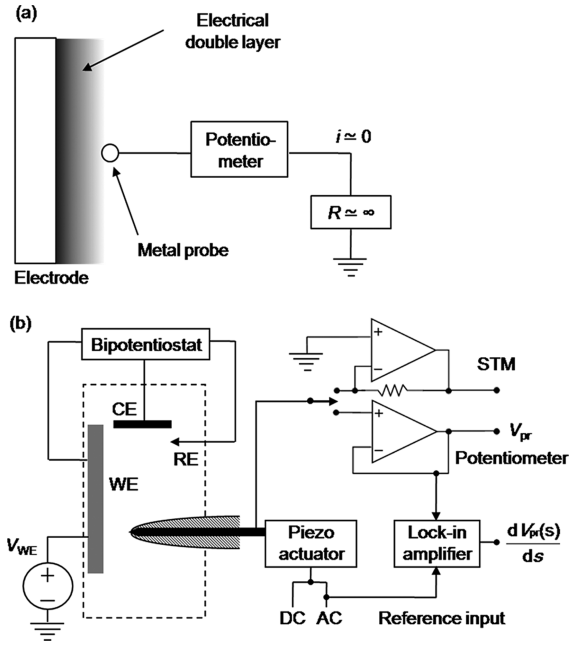

Figure 1. (a) Concept of EDL potential measurement with an ideal potential probe. (b) Schematic drawing of the experimental setup. In an electrochemical cell depicted by the dashed-line box, a nanometer-sized potential probe approaches the working electrode (WE) surface and monitors the local potential of solution inside the gap between the probe and the WE. The potential at the probe (V_{pr}) is measured with a voltage follower accessed by switching from STM mode. To measure the potential gradient (dV_{pr}/ds), the probe is oscillated back and forth, and the induced potential modulation is measured through a lock-in amplifier.

negligible specific adsorption onto gold surfaces,[4b] which simplifies the electrochemical interface structure of the gold electrodes in the solution.

An important part of the experiment was the preparation of a miniaturized potential probe. To measure the EDL potential at the intended spatial resolution, the maximum extension of the gold apex protruding from the insulating sheath must be sufficiently smaller than the decay length of the EDL. Theoretical simulations[17] predict that a lower height apex produces a potential curve closer to the actual potential profile of the EDL. We reduced the gold apex height by using the method of ultrashort (<50 ns) pulse etching,[20] after the initial preparation of the probe with an insulator film coating. The progressive reduction of the apex size by the pulse etching produced a nanometer electrode with a disk-shaped surface and a small vertical protrusion.[20] The size of the electrode thus prepared was typically ∼10 nm in radius assuming a disk shape, as estimated from cyclic voltammetry (CV) experiments for the $Fe(CN)_6^{3-}/Fe(CN)_6^{4-}$ redox reaction.[20] Even though pulse etching greatly improved the success rate of producing a disk-shaped nanometer probe, the probes thus prepared had to be tested for the potential profiling experiment before final selection. The preparation method of a nanometer potential probe has been described in detail eleswhere.[20,30]

The potentiometer was constructed using an operational amplifier with ultrahigh input resistance (LMC6001AIN, National Semiconductor, leakage current ≤ 10 fA at 25 °C) and wiring the electronic components directly to the operational amplifier through air to reduce the leakage current.[15] The characteristics

of the potential probe and the potentiometer used in the measurement of the electrochemical potential of solution were described previously.[15] The characterization method of the system involved a dynamic response measurement for the solution potential changing as a step function. The dynamic response curves gave information about the interfacial impedance of the probe and the input impedance of the potentiometer. Typically, a probe having a gold apex size of ~100 nm in radius exhibited an interfacial resistance of $\sim 10^{12}$ Ω in $NaClO_4$ aqueous solution.[15] The potentiometer input impedance was $\sim 10^{13}$ Ω.

The movement of the probe was driven by a piezo actuator and an STM controller (RHK Technology Inc.). The probe, initially located at a tunneling distance from the WE surface in STM mode, was retracted to a distance far enough to completely escape from the EDL at the WE. Then, the probe was switched from the current reading mode (STM) to the potential reading mode (potentiometer) and remained in the solution bulk position for ~20 s to ensure that the probe potential was stabilized. A potential profiling experiment started from this position by slowly advancing the probe toward the WE surface until contact was made with the surface, and then the probe was moved away from the WE to the bulk position. In this way, the probe read the potential of the local solution environment as a function of the distance between the probe and the WE. An alternative experiment involved the measurement of the potential gradient by modulating a gap distance. An ac voltage was applied to the piezo drive so that the probe oscillated back and forth in small amplitudes ($\Delta s \leq 1$ nm) in a direction normal to the WE surface. The oscillation frequency was 10−20 Hz, which was within the bandwidth (≤100 Hz) of the potential probe system. The induced potential modulation due to the probe oscillation was measured using a lock-in detection technique and converted into the potential gradient of the local environment. The potential and potential gradient signals were simultaneously recorded as the probe was moving slowly along the perpendicular direction to the WE surface, thereby giving the potential and potential gradient profiles as a function of the gap distance. Control experiments revealed that the potential profile shape was unaffected by the probe vibrations in small amplitudes. A complete profile required 1−20 s depending on the linear traveling speed of the probe. The lowest profiling speed was limited by the instrumental thermal drift (≤0.2 nm s^{-1}) in the gap distance.

3. RESULTS AND ANALYSIS

Figure 2 shows an example of the results of potential and potential gradient profile measurements. In this experiment, a potential probe approached the WE surface in a 10 mM $NaClO_4$ solution until electrical contact was made between the probe and the WE and then retracted from the WE surface to a position in the bulk solution. During the approach and retraction motions, the potential (V_{pr}) and potential gradient (dV_{pr}/ds) signals were simultaneously monitored at the probe. We first discuss the V_{pr} curve obtained during the approach. The curve shows features that are qualitatively similar to those observed in previous studies.[13,14] For example, at a sufficiently long distance from the WE, the probe read a constant potential corresponding to the open-circuit potential (ocp) of the solution, V_{bulk}. The ocp value measured with the probe was somewhat shifted from that measured with a large gold electrode, and the difference was

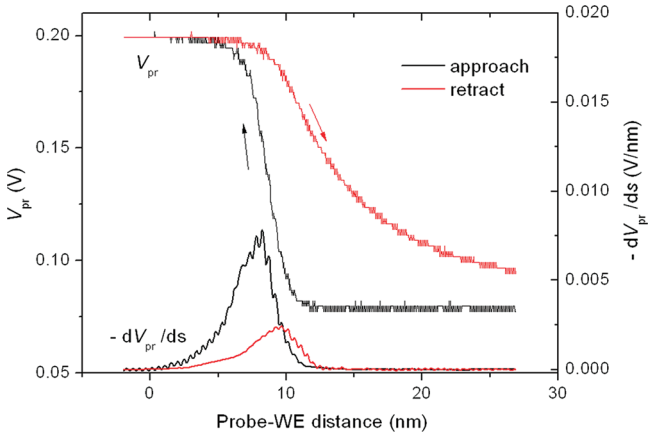

Figure 2. V_{pr} and dV_{pr}/ds signals measured as a function of the distance between a probe and a WE. The probe moved toward (black line) and away from (red line) the WE surface ($s = 0$ nm) at a linear translation speed of 5 nm s^{-1} in a 10 mM $NaClO_4$ solution. The probe oscillation frequency was 10 Hz, and the oscillation amplitude (Δs_{rms}) was 0.57 nm. The dV_{pr}/ds curve had tiny ripples superimposed onto it, which resulted from the coupling of the linear and oscillatory motions of the probe (see text). V_{WE} was 0.2 V with respect to the ground (E_{WE} was 0.15 V vs gold quasi-RE, which corresponded to ~0.48 V vs Ag/AgCl RE). The size of the gold probe was ~20 nm in radius assuming a disk-shaped surface.

explained by the large interfacial resistance of the nanometer probe.[15] As the probe approached the WE surface, V_{pr} gradually changed toward the bias potential of the WE (V_{WE}). The variation in V_{pr} in this region reflected the potential distribution in the gap between the WE and the probe. At close gap distances, the slope of the curve gradually decreased to a sigmoidal shape. This feature made it difficult to identify the exact probe−WE contact position in the curve, which did not show any discernible discontinuity due to the contact. In the figure, we marked the contact position ($s = 0$) as it was deduced according the curve analysis described later in this section.

When the probe retracted from the WE surface to the solution bulk, the potential reading changed gradually from V_{WE} toward V_{bulk}. However, the potential curves exhibited a strong hysteresis, such that V_{pr} did not quickly revert to the V_{bulk} value along the retract motion, compared to the time that it took for V_{pr} to reach the V_{WE} value during the approach. For example, in Figure 2, V_{pr} did not fully drop to V_{bulk} until the retraction scan ended, which took 6 s (equivalent to a distance of 30 nm). The hysteresis effect was even more pronounced for a faster profiling experiment, indicating that the hysteresis depended on the time of the measurement rather than the location. In principle, the hysteresis effect could be removed by measuring the potential profile infinitely slowly. This, however, was practically impossible because of the instrument thermal drift, which changed the gap distance with time. It was obvious that an alternative experimental method was needed to remove the problematic hysteresis from the measured potential profile. This method is described below.

The potential gradient (dV_{pr}/ds) curves obtained from the distance-modulation experiments are also displayed in Figure 2. The dV_{pr}/ds profiling experiments produced a bell-shaped curve, with tiny periodic ripples superimposed onto it. The ripples were part of dV_{pr}/ds signals rather than noises. The ripples appeared because the speed of the probe vibrational motion (ds/dt) differed in the forward and backward directions as a result of the addition (or subtraction) of the linear translational speed of

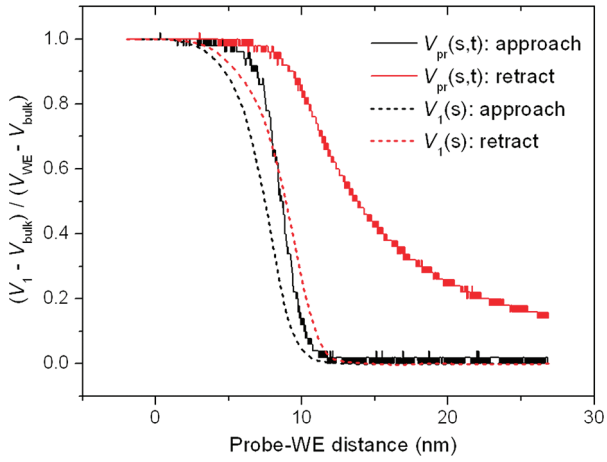

Figure 3. Plot of the distance-dependent potential component $[V_1(s)]$ of the probe signal $[V_{pr}(s,t)]$ as a function of gap distance (dotted lines). The $V_1(s)$ profilesweare obtained through the integration of the dV_{pr}/ds curves shown in Figure 2, and they are displayed on the normalized scale $(V_1 - V_{bulk})/(V_{WE} - V_{bulk})$ (see text). The experimental V_{pr} curves (solid lines) are also shown for comparison.

the probe. The ripples should not be misinterpreted as interfacial potential oscillations with distance. First, we discuss some qualitative features of the V_{pr} and dV_{pr}/ds curves that can be noticed from a simple visual survey of the curves. When we compare the V_{pr} and $|dV_{pr}/ds|$ curves for the approach scan, the maximum in $|dV_{pr}/ds|$ appeared at a position near the steepest slope in the V_{pr} curve, as expected for the derivative of a sigmoidal V_{pr} function. For the retract scan, however, the $|dV_{pr}/ds|$ profile showed a maximum at a distance of 9−10 nm, which was markedly different from the position of the steepest slope in the corresponding V_{pr} curve. In addition, the $|dV_{pr}/ds|$ signal dropped almost to zero at a distance of ∼13 nm, even though the corresponding V_{pr} curve did not plateau out at farther distances. Importantly, however, the dV_{pr}/ds curves had approximately the same width for the approach and retract scans, although their relative peak positions were shifted and the heights were different. This feature was verified by conducting dV_{pr}/ds measurements at different linear scan speeds, which showed that the width of the dV_{pr}/ds curves was approximately constant independent of the scan speed, albeit the corresponding V_{pr} curves exhibited stronger hysteresis for a faster scan (Supporting Information). These observations indicated that the time-dependent hysteresis in V_{pr} curves was attenuated in dV_{pr}/ds measurements. In the following discussion, we analyze the different features between V_{pr} and dV_{pr}/ds curves in further detail.

The dV_{pr}/ds signal contains information only about the potential change associated with a change in probe−surface distance but excludes the time-dependent component in the potential measurement. Suppose that the potential measured at the probe results from the superposition of two different potentials, one that varies with distance $[V_1(s)]$ and the other that varies with time $[V_2(t)]$. Then, the probe signal is expressed as a weighted average of $V_1(s)$ and $V_2(t)$

$$V_{pr}(s,t) = \frac{R_1 V_2(t) + R_2 V_1(s)}{R_1 + R_2} \quad (1)$$

where R_1 and R_2 are resistors connected in parallel to the $V_1(s)$ and $V_2(t)$ sources, respectively. Here, we use the potential and voltage in interconvertible meaning to indicate the probe signal.

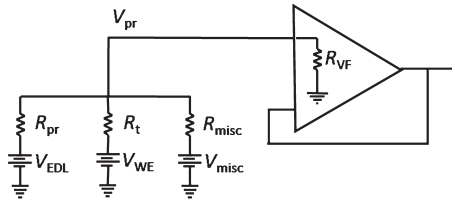

Figure 4. Equivalent circuit of the system involved in the potential profiling experiments.

The distance-modulation experiment extracts only the $V_1(s)$ component from the $V_{pr}(s,t)$ signal through differentiation with respect to distance

$$\left.\frac{dV_{pr}(s,t)}{ds}\right|_{t=\text{const}} = \left(\frac{R_2}{R_1 + R_2}\right)\frac{dV_1(s)}{ds} \quad (2)$$

Integration of the $dV_{pr}(s,t)/ds$ signal over the distance can restore $V_1(s)$, which is the potential profile as a function of gap distance. Figure 3 shows $V_1(s)$ profiles thus obtained from the dV_{pr}/ds curves presented in Figure 2. Because the dV_{pr}/ds curves have different bell-shaped areas for the approach and retract scans, the integration produces sigmoidal $V_1(s)$ curves with different potential heights. As explained later using the equivalent circuit model analysis, this is because the dV_{pr}/ds measurements provide information only about the relative potential variation as a function of distance, rather than the absolute potential height. Nonetheless, we display the $V_1(s)$ curves on a normalized scale in Figure 3, such that $(V_1 - V_{bulk})/(V_{WE} - V_{bulk})$ changes from zero in the solution bulk to unity at the probe−surface contact, for the purpose of comparing the width of the curves only. This normalization procedure is justifiable because it is physically obvious that the interfacial potential profile spans from V_{WE} at the electrode surface to V_{bulk} in the bulk position. Another feature is that the integration removes the ripples in the dV_{pr}/ds curves and produces unwrinkled sigmoidal $V_1(s)$ curves even without curve smoothing [the $V_1(s)$ curves contain only "integrated ripples"]. As Figure 3 shows, the $V_1(s)$ curves for the approach and retract scans resemble each other closely in their width and sigmoidal curve shapes after the normalization, indicating that the time-dependent hysteresis disappears in the $V_1(s)$ curves. However, the two $V_1(s)$ curves appear shifted by ∼2 nm in their relative position. This amount of shift might occur as a result of the instrumental thermal drift and/or mechanical distortion of the probe−WE junction upon contact. Note that these instrumental factors result in a nominal shift in gap distance. That is, the shift occurs in the reference position rather than in the actual gap distance. Admitting this possibility, we can neglect the ∼2-nm shift in the $V_1(s)$ curves and would then find that they overlap with each other very well.

In the following discussion, we explain the conversion procedure of $dV_{pr}(s,t)/ds$ to $V_1(s)$ in detail. For this purpose, the potential probe system is analyzed in terms of a relevant equivalent circuit model. The equivalent circuit for the system is shown in the diagram of Figure 4. The electrochemical environment acting on the probe during the potential reading is simulated by introducing three external voltage sources, which are connected to the probe through three parallel resistors. These voltage sources include (i) the potential distribution of EDLs in the gap (V_{EDL}), where V_{EDL} is transmitted to the probe through the solution/gold interface at the probe apex, which has an

interfacial resistance of R_{pr};[15] (ii) the voltage applied at WE (V_{WE}), which, at a close gap distance, leaks into the probe due to electron tunneling[21] [although V_{WE} is a constant voltage, the tunneling resistance (R_t) varies with the gap distance, and therefore, the contribution of V_{WE} to V_{pr} varies with distance]; and (iii) miscellaneous voltages (V_{misc}), which influence the probe potential through routes other than potential sensing mechanisms I and ii. V_{misc} could have multiple sources. For example, because the probe is covered with a polymer film whose surface area is huge compared to the exposed gold surface, the probe potential might be affected by the potential sensing in the film-coated region, such as percolation of ions through pinholes and slits possibly present in the thin polymer coating near the gold apex. Moreover, the electrochemical equilibrium between the polymer sheath and the electrolyte solution might respond to the field gradient in the EDL. The dielectric charging and relaxation of polymer molecules at the metal/polymer interface might also affect the potentiometric response. The electrolyte percolation through the hydrophobic polymer is predicted to be slow,[22] and so is the dielectric relaxation of the polymer.[23] Therefore, these processes might affect the probe potential slowly during the potential profiling experiments, producing the hysteresis in the V_{pr} curves. Such miscellaneous voltage sources are simulated by introducing V_{misc} and R_{misc} into the equivalent circuit. The probe measures the weighted average of V_{EDL}, V_{WE}, and V_{misc} through a voltage follower with input resistance R_{VF}. Here, we neglect EDL capacitance in the equivalent circuit analysis because the response time of EDL to the external perturbation in the localized area is much faster (less than or equal to microseconds) than the probe oscillation period (~0.1 s),[20,24] and therefore, the EDL relaxation process will not act as impedance in the distance-modulation experiment. Other capacitive contributions to the measurement such as the dielectric relaxation of the polymer are also neglected based on the notion that these processes occur very slowly[23] compared with the probe oscillation period.

For the equivalent circuit shown in Figure 4, the potential read at the probe is expressed by the equation

$$V_{pr} = \frac{R_{VF}(R_{pr}R_tV_{misc} + R_tR_{misc}V_{EDL} + R_{misc}R_{pr}V_{WE})}{R_{pr}R_tR_{misc} + R_tR_{misc}R_{VF} + R_{misc}R_{VF}R_{pr} + R_{VF}R_{pr}R_t} \quad (3)$$

The three voltage sources influence V_{pr} in different ways. The contributions of V_{EDL} and V_{WE} to V_{pr} are functions of the gap distance. The time-dependent change of V_{pr} is attributed to V_{misc}, which includes potential changes due to the interactions of a polymer film with electrolyte solution and the dielectric response of the polymer. The dV_{pr}/ds expression derived from eq 3 is difficult to integrate analytically. Therefore, we consider dV_{pr}/ds for two limiting cases: (i) a long-distance region where electron tunneling is negligible and (ii) a short-distance region where the tunneling effect is dominant. According to a one-dimensional tunneling equation, the electron tunneling resistance varies with gap distance as $R_t = R_0 \exp(s/a)$, where R_0 is the resistance at the contact point and a is the decay length of the electron tunneling probability in solution. Typical values for these parameters are $R_0 = 5 \times 10^4\ \Omega$ for a contact between a gold tip and a gold surface and a = 0.10−0.15 nm in aqueous solutions of 1−100 mM $NaClO_4$ concentration and for a junction voltage of 0.1 V.[21] According to these values, R_t exceeds R_{pr} (~$10^{12}\ \Omega$) when the gap distance is longer than 3 nm. Owing to the exponential increase of R_t with distance, V_{pr} is contributed mostly by V_{EDL} and V_{misc} beyond this distance. The dV_{pr}/ds expression derived from eqs 2 and 3 for this limiting case ($R_t \rightarrow \infty$) is

$$\left.\frac{dV_{pr}(s,t)}{ds}\right|_{t=\text{const}} \approx \left(\frac{R_{VF}R_{misc}}{R_{pr}R_{misc} + R_{misc}R_{VF} + R_{VF}R_{pr}}\right)\frac{dV_{EDL}(s)}{ds} \quad (4)$$

Equation 4 shows that the dV_{pr}/ds measurement in the long-distance region gives information exclusive to dV_{EDL}/ds. The analysis is made under the assumption that V_{misc} varies only with time but not with distance. This assumption, however, might not be entirely correct, if V_{misc} depends also on the probe location inside an EDL because V_{misc} includes the effects of the polymer−electrolyte interactions. Even in this case, the resulting change in V_{misc} might occur only slowly, as mentioned above. The ac-modulation experiment then acts as a high-pass filter, which removes the V_{misc} signals that change slowly compared to the mechanical oscillation frequency of a probe. On the other hand, the signal due to the EDL potential (dV_{EDL}/ds) transmits properly through the high-pass filter because the EDLs respond instantaneously (less than or equal to microseconds) to the external perturbation of probe oscillation. As a result, the modulation experiment extracts V_{EDL} but filters out V_{misc} by detecting high-frequency dV_{pr}/ds signals that correspond to dV_{EDL}/ds. Integration of the dV_{EDL}/ds signal over distance then restores the V_{EDL} profile.

In the short-distance tunneling regime, where R_t is negligibly small compared with R_{pr}, R_{VF}, and R_{misc}, eq 3 can be approximated as

$$V_{pr} \approx V_{WE}\left(1 - \frac{R_t}{R_{pr} + R_{misc} + R_{VF}}\right) \quad (5)$$

Because R_t varies exponentially with gap distance, V_{pr} is almost constant and equal to V_{WE} for $s < 2$ nm. The contribution of V_{WE} to V_{pr} rapidly drops to zero for $s > 3$ nm. Owing to such a drastic change over a narrow distance range, the contribution of V_{WE} to V_{pr} behaves almost like a step-function.

As shown in Figure 2, the distance-modulation experiments produce dV_{pr}/ds curves with different bell-shaped areas for approach and retract scans. Consequently, these dV_{pr}/ds curves are integrated into sigmoidal V_{pr} curves of different potential heights. The reason a dV_{pr}/ds curve is different for approach and retract scans is as follows: According to eq 4, the linear proportionality constant between the measured $dV_{pr}(s, t)/ds$ signal and the true potential gradient (dV_{EDL}/ds) is determined by a combination of R_{misc}, R_{VF}, and R_{pr} values. This effect can be illustrated, for example, by considering a situation that the time-dependent hysteresis appears strongly along the retract motion right after the probe−WE contact. It corresponds to the condition that V_{misc} is relatively large or R_{misc} is small. Dielectric charging at the Au−polymer interface during a probe−WE contact might be able to generate such a condition. In this case, a small R_{misc} value will produce a weak dV_{pr}/ds signal (eq 4), and this prediction agrees with the experimental observation. Related to this explanation, Figure 2 shows that the height of a dV_{pr}/ds curve does not precisely match the graphic slope of the corresponding V_{pr} curve. This mismatch is attributed to the fact that the weight factors for three voltage contributions (V_{EDL}, V_{WE}, and V_{misc}) are different for V_{pr} and dV_{pr}/ds signals, as shown in eqs 3 and 4. Also, there can be an extra instrumental factor because the dV_{pr}/ds signal intensity measured by a phase-sensitive

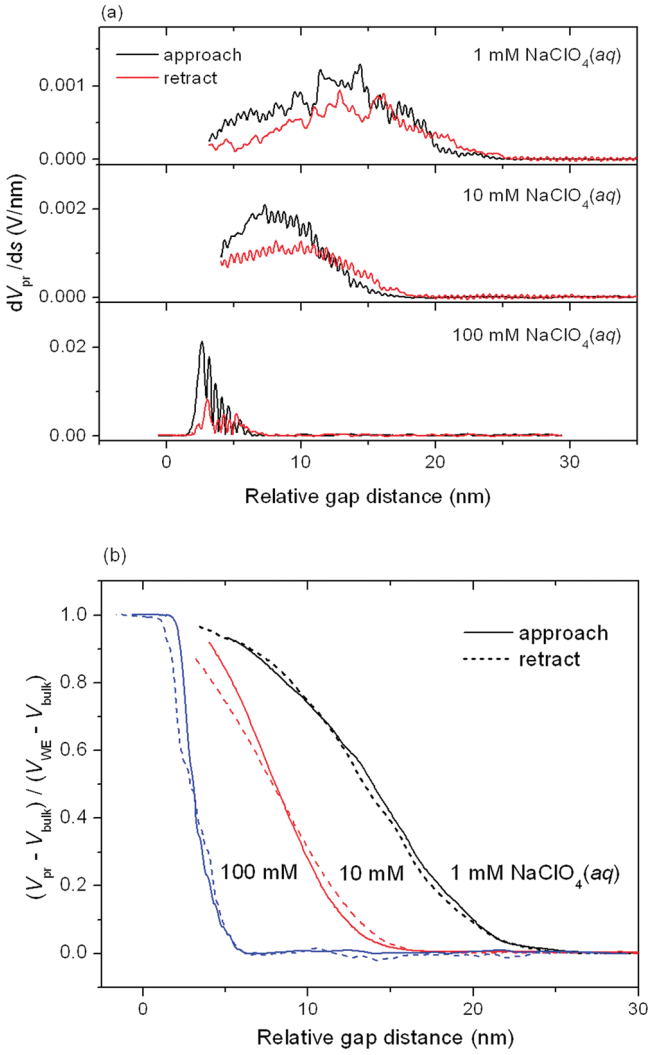

Figure 5. (a) Potential gradient (dV_{pr}/ds) curves measured as a function of gap distance in 1.0, 10, and 100 mM $NaClO_4$ solutions. The linear translational speed of the probe was 5 nm s^{-1}. The probe oscillation frequency was 10 Hz. The oscillation amplitude (Δs_{rms}) was 0.58 nm for the 1.0 and 10 mM solutions and 0.033 nm for the 100 mM solution. The ripples were strong in the 100 mM curves because the ds/dt value differed greatly in the forward and backward vibrations due to comparable speeds of the linear translational and vibrational motions of the probe. (b) Potential profiles [$V_{pr}(s)$] converted from the experimental dV_{pr}/ds curves, displayed on the normalized scale $(V_{pr} - V_{bulk})/(V_{WE} - V_{bulk})$, after correction of the distance shift (see text). V_{WE} was 0.2 V.

detection method can change with the lock-in amplifier parameter. Although one can determine the R_{pr} and R_{VF} values by conducting calibration experiments for the potential probe system,[15] the R_{misc} value and its changing behavior during the profiling experiments are unknown. For this reason, distance-modulation experiments can measure only the *relative* potential variation as a function of distance rather than the *absolute* potential height.

Figure 5a shows results of potential gradient measurements in $NaClO_4$ solutions of various concentrations. The measurements were made in the sequence of 1.0, 10, and 100 mM solutions. As can be seen in the figure, the probe did not fully touch the WE surface in the experiments with 1.0 and 10 mM solutions, and it made a firm mechanical contact with the WE only during the last approach in the 100 mM solution. Therefore, the probe apex structure was probably preserved without significant damage in the 1.0 and 10 mM experiments before the final contact was made in the 100 mM solution. The results show that the width of the dV_{pr}/ds curve decreases as the $NaClO_4$ concentration increases. This indicates a trend for the potential profile in the gap to become steeper at higher electrolyte concentrations.

The dV_{pr}/ds curves were converted into V_{pr} curves according to the procedures described above, and the results are shown in Figure 5b. In the figure, the V_{pr} curves for the approach and retract scans are shown overlapping for each set of data; this is done by correcting the nominal shift in gap distance due to instrumental drift, mentioned above. The probe−WE contact position is not clearly identifiable in the experimental curves. Based on the curve analysis with the equivalent circuit model, we conclude that the contact occurs at the position of ∼1.9 nm toward the WE from the position where the V_{pr} profile reaches the full value (≥0.99) of V_{WE}; this extra distance accounts for the electron tunneling region. Owing to the uncertainty in this contact position assignment, the gap distance in the figure can be regarded as an approximate measure. The resulting V_{pr} curves for the approach and retract experiments overlap nicely with each other after the correction of the shift. This indicates that the distance-modulation experiment removes the time-dependent hysteresis and produces a more reproducible potential profile than the direct measurement of V_{pr} does, where the measured potential profile changes with scan speed and other temporal factors. Because electron tunneling does not significantly contribute to V_{pr} for $s >$ 3 nm, the V_{pr} curve features in this region represent exclusively the contribution of the EDL potentials in the gap.

4. DISCUSSION

The V_{pr} profiles obtained from the distance-modulation experiments show that the profile becomes broader as the electrolyte concentration decreases (Figure 5b). This general trend agrees with the dependence of the diffuse double-layer thickness on electrolyte concentration. When the shape of the potential profiles is compared, the tail part of the observed V_{pr} profile resembles the potential distribution of a diffuse double layer in the Gouy−Chapman (G−C) model, which shows an exponential decay with distance. At closer distances, however, the shape of the experimental curve is significantly different from that of the G−C model. Theoretical models predict that the potential in a diffuse double layer should exhibit a steeper slope toward the electrode surface and then linearly increase in the Stern layer.[1−4] The experimental curves show an inflection point and then a sigmoidal bending toward the WE without a discernible break at the contact point. The difference can be attributed to the fact that the present experiment measures the interfacial potential in the gap between the probe and WE surfaces, rather than the potential of the EDL at an isolated electrode surface. Detailed theoretical analysis of the potential profiles measured in SECPM experiments has been reported by Hamou et al.[16,17] These studies show that the EDLs located at the probe and the electrode overlap during the approach, as expected, and the observed potential profiles are a result of the interactions of the EDLs. In this case, the unperturbed EDL potential can be extracted only through the deconvolution of the experimentally observed potential profile. Such a deconvolution analysis would require detailed information about the EDL structure at the probe and WE, which is difficult to ascertain at present.

Table 1. Decay Length of Diffuse Double Layer, $1/\kappa$ (nm), Estimated from the LSA Analysis of V_{pr} Curves and the G−C Model

	electrolyte concentration		
	1 mM	10 mM	100 mM
V_{pr} curve	3.1 ± 1.5	1.8 ± 0.9	0.9 ± 0.9
G−C model*	9.62	3.04	0.96

* Calculated for ε = 78.5 and T = 298 K.

Nevertheless, we can attempt to analyze the experimental V_{pr} curves by assuming that the linear superposition approximation (LSA) holds for the EDL interaction. In the LSA, the interfacial potential constructed from two weakly interacting EDLs is represented as a linear superposition of the potentials of two independent EDLs.[25] In this case, the change in the probe potential along the movement of the probe strace the potential profile of the EDL at the WE.[13] This is a good approximation when the EDL on the probe surface is very weak, according to the theoretical simulations of overlapping EDLs.[17] We have assumed that the EDL interaction is weak enough to apply the LSA at sufficiently long distances corresponding to the tail part of the experimental V_{pr} curves, where $(V_{pr} - V_{bulk})/(V_{WE} - V_{bulk}) < 0.05$, and analyzed the curves only for this region. According to the G−C model, the potential distribution of a diffuse double layer composed of 1:1 electrolytes is described by

$$\tanh(eV_{pr}/4kT)/\tanh(eV_{WE}/4kT) = \exp(-\kappa x) \quad (6)$$

where V_{pr} is the potential relative to the bulk solution at distance x from WE and κ is the reciprocal of the characteristic thickness of a diffuse double layer. κ is estimated from the slope of the linear plot of $\ln[\tanh(eV_{pr}/4kT)/\tanh(eV_{WE}/4kT)]$ versus s. Table 1 lists the decay length $(1/\kappa)$ of a diffuse double layer estimated from the V_{pr} curves shown in Figure 5b. The measured decay length might have uncertainties arising from the assumptions used in the curve analysis, as well as the instrumental spatial resolution. We estimated the instrumental resolution by assuming that it is equal to the width of the narrowest potential profile that can be resolved with the instrument. The potential profile curves used for this purpose in the data set of Figure 5 are those measured at 100 mM concentration, which show a decay length of $1/\kappa$ = 0.9 nm. The experimental uncertainty thus estimated (±0.9 nm) is added to the error bars of the other potential profile data. This procedure might suggest a reasonable uncertainty limit for the potential profiles at lower concentrations, although we lose physical significance of the data point at 100 mM ($1/\kappa$ = 0.9 ± 0.9 nm at 100 mM).

The experimental decay length increases from 1.8 ± 0.9 nm at 10 mM to 3.1 ± 1.5 nm at 1.0 mM. The data are at least consistent with the proportionality of the decay length to the inverse square root of electrolyte concentration predicted by theories, although the large uncertainty in the data set clouds the quantitative verification of this relationship. It can be noticed that the experimental decay length is shorter than the G−C value (Table 1). Such disagreement might not be unexpected, considering many differences between the present experiment, measuring the potential inside the gap with a nonideal potential probe, and the simplified G−C model of an isolated EDL. Also, the Debye screening effect might reduce the decay length of the measured potential profiles.[14,16,17] In addition, one might question the validity of the LSA used for the analysis[25] and the dielectric permittivity of the electrolyte medium used for the G−C model. The theoretical decay length was calculated assuming a uniform dielectric background (ε = 78.5) in a diffuse double layer. However, it is well-known[26−28] that dielectric saturation near the electrode surface can reduce the dielectric permittivity of the interfacial water molecules depending on their location, and this effect can significantly alter the potential profile compared to the prediction of the simple model.[28] Incidentally, when the values for the variable ε reported by Teschke et al.[27] are incorporated into the G−C model, the calculated decay length becomes much closer to our experimental value.[29] Thus, it appears that a naïve comparison of the experimental results with theoretical models could lead to a misleading conclusion, until both experiment and theory are further developed.

5. CONCLUSIONS

This work demonstrates that the distance-modulation method of detecting the potential gradient signal can measure the variation of the interfacial potential as a function of gap distance. The method exclusively measures the contribution of EDL potentials in the gap through the detection of high-frequency dV_{pr}/ds signals. At the same time, it filters out time-dependent noises and slow hysteresis which are possibly related to the use of a potential probe of complicated apex structure constructed with a metal tip and polymer sheath. As such, the method can measure the width of the potential profile more accurately than the direct potential reading method does, although it cannot quantitatively measure the absolute potential height . The distance-modulation method is expected to be applicable to SECPM experiments as well, offering an alternative method for electrochemical potential imaging of surfaces using the potential gradient as a feedback signal.

The observed interfacial potential profiles show an exponential decay in the tail region, where the interaction between the EDLs present on the probe and WE surfaces is very weak. At closer gap distances, the potential profiles exhibit an inflection point and then a sigmoidal bending toward the WE potential, and these features might differ from the potential distribution of an isolated EDL on an electrode surface. These features might arise from several factors, including the overlapping of the EDLs on the probe and WE surfaces, as well as electron tunneling between the two surfaces at very close distances. Quantitative understanding of the observed potential profiles in terms of individual EDL components on the probe and WE surfaces will require further theoretical work. Also, technical advances in the preparation of a nanometer potential probes will be important in future studies to monitor the electrolyte/electrode interface with minimal disturbance.

■ ASSOCIATED CONTENT

Supporting Information. Potential and potential gradient curves measured at different linear scan speeds of the probe. This information is available free of charge via the Internet at http://pubs.acs.org.

■ AUTHOR INFORMATION

Corresponding Author

*E-mail: surfion@snu.ac.kr (H.K.), tdchung@snu.ac.kr (T.D.C.). Fax: +82 2 889 1568.

Present Addresses
[†]Present address: Samsung Electronics, Giheung-Gu, Youngin, Gyeonggi-Do 446-711, Republic of Korea.

ACKNOWLEDGMENT

This work was supported by a National Research Foundation grant funded by the Korea government (MEST) (2011-0001219).

REFERENCES

(1) Gouy, G. *J. Phys. (Paris)* **1910**, *9*, 457.
(2) Chapman, D. L. *Philos. Mag.* **1913**, *25*, 475.
(3) Stern, O. *Z. Elektrochem.* **1924**, *30*, 508.
(4) (a) Grahame, D. C. *Chem. Rev.* **1947**, *41*, 441. (b) Parsons, R. *Chem. Rev.* **1990**, *90*, 813.
(5) Israelachvili, J. N.; Adams, G. E. *J. Chem. Soc., Faraday Trans. I* **1978**, *74*, 975.
(6) Pashley, R. M. *J. Colloid Interface Sci.* **1981**, *83*, 531.
(7) Ducker, W. A.; Senden, T. J.; Pashley, R. M. *Nature* **1991**, *353*, 239.
(8) Ishino, T.; Hieda, H.; Tanaka, K.; Gemma, N. *Jpn. J. Appl.Phys.* **1994**, *33*, L1552.
(9) Hillier, A. C.; Kim, S.; Bard, A. J. *J. Phys. Chem.* **1996**, *100*, 18808.
(10) Corbella, C.; Pascual, E.; Oncins, G.; Canal, C.; Andujar, J. L.; Bertran, E. *Thin Solid Films* **2005**, *482*, 293.
(11) Baier, C.; Stimming, U. *Angew. Chem., Int. Ed.* **2009**, *48*, 5542.
(12) Wolfschmidt, H.; Baier, C.; Gsell, S.; Fischer, M.; Schreck, M.; Stimming, U. *Materials* **2010**, *3*, 4196.
(13) Woo, D. H.; Yoo, J. S.; Park, S. M.; Jeon, I. C.; Kang, H. *Bull. Korean Chem. Soc.* **2004**, *25*, 577.
(14) Hurth, C.; Li, C.; Bard, A. J. *J. Phys. Chem. C* **2007**, *111*, 4620.
(15) Yoon, Y. H.; Shin, T.; Shin, E. Y.; Kang, H.; Yoo, J. S.; Park, S. M. *Electrochim. Acta* **2007**, *52*, 4614.
(16) Hamou, R. F.; Biedermann, P. U.; Erbe, A.; Rohwerder, M. *Electrochem. Commun.* **2010**, *12*, 1391.
(17) Hamou, R. F.; Biedermann, P. U.; Erbe, A.; Rohwerder, M. *Electrochim. Acta* **2010**, *55*, 5210.
(18) Dickinson, E. J. F.; Compton, R. G. *J. Phys. Chem. C* **2009**, *113*, 17585.
(19) Clavilier, J.; Faure, R.; Guinet, G.; Durand, R. *J. Electroanal. Chem.* **1980**, *107*, 205.
(20) Woo, D. H.; Kang, H.; Park, S. M. *Anal. Chem.* **2003**, *75*, 6732.
(21) Woo, D. H.; Choi, E. M.; Yoon, Y. H.; Kim, K. J.; Jeon, I. C.; Kang, H. *Surf. Sci.* **2007**, *601*, 1554.
(22) Morf, W. E. *The Principles of Ion-Selective Electrodes and of Membrane Transport*; Elsevier Science: Amsterdam, 1981; Chapter 10.
(23) Anthony, R.; Jones, L.; Richards, R. W. *Polymers at Surfaces and Interfaces*; Cambridge University Press: Cambridge, U.K., 1999; Chapter 1.
(24) Feldberg, S. W. *J. Phys. Chem.* **1970**, *74*, 87.
(25) Verwey, E. J. W.; Overbeek, J. Th., G. *Theory of the Stability of Lyophoic Colloids*; Elsevier: Amsterdam, 1948.
(26) Grahame, D. C. *J. Chem. Phys.* **1950**, *18*, 903.
(27) (a) Teschke, O.; Ceotto, G.; de Souza, E. F. *Chem. Phys. Lett.* **2000**, *326*, 328. (b) Teschke, O.; Ceotto, G.; de Souza, E. F. *Phys. Rev. E* **2001**, *64*, 011605.
(28) Kornyshev, A. A.; Kuznetsov, A. M. *Electrochem. Commun.* **2006**, *8*, 679.
(29) Woo, D. H. Direct Probing of the Electrified Interfaces with a Potential Nano-Probe: The Potential Profile of Electric Double Layers. Ph.D Thesis, Pohang University of Science and Technology, Pohang, South Korea, 2004.
(30) Lee, S. K.; Yoon, Y. H.; Kang, H. *Electrochem. Commun.* **2009**, *11*, 676.